Time evolution of the electric field – Part 1: using the rapid expansion method (REM) with pseudo-spectral evaluation of spatial derivatives

Time evolution of the electric field – Part 1: using the rapid expansion method (REM) with pseudo-spectral evaluation of spatial derivatives

Paul L. Stoffa[1] and Anton Ziolkowski[2]*
[1]University of Texas at Austin, Institute for Geophysics and Department of Geological Sciences, Jackson School of Geological Sciences, Austin, Texas, USA. [2]University of Edinburgh, School of Geosciences, Edinburgh, UK.

Summary

We present a method for modeling transient EM data acquired on land or at sea. We use the rapid expansion method (REM) to develop the 3-component electric wave field time response from the spatial responses found using a pseudo-spectral method. The results are free of numerical dispersion and accurate to the Nyquist frequency in time and space. The resulting diffusive field is a weighted sum of Chebyshev polynomials, which exhibit a wave-like character and are very sensitive to small perturbations in the medium. The method is intrinsically parallel which leads to computational efficiency. Numerical results compare favorably with the analytic response and 1D methods even though the computations are intrinsically 3D.

Introduction

Low frequency electromagnetic (EM) modeling in conducting media has become especially important in the last fifteen years during which there has been a rapid development of the controlled source electromagnetic (CSEM) method. Unlike the seismic method, there is no ray theory for EM, and interpretation of the data is totally dependent on the accuracy of the modeling. Mittet (2010) provides an excellent overview of finite-difference time domain approaches to the problem of modeling EM data and analyzes the trade-off between speed and accuracy before proposing his own improved finite-difference approach. All finite-difference schemes have accuracy limited by the approximations of the spatial and temporal derivatives.

We solve for the 3D three-component E-field directly using an explicit time evolution called the rapid expansion method (REM), proposed by Tal-Ezer (1986, 1989), combined with a pseudo-spectral evaluation for the spatial derivatives (Fornberg, 1987; Fornberg, 1988). Our method is based on an approach proposed by Carcione (2006), who solved the 2D problem for a magnetic source. Pestana and Stoffa (2010) have applied REM to the time evolution of the 3D acoustic wave equation. Unlike finite difference methods, our method is accurate to the Nyquist frequency in time and the Nyquist wavenumber in space. Further, the method is unconditionally stable. We incorporate the analytic solution for an impulsive electric dipole source in a full space as our initial condition to begin the time evolution of the 3D three-component E-field. The REM expands the exponential of the spatial operator using Chebyshev polynomials, which possess a wave-like character that shows where the energy is propagating. After the integration of the polynomials with modified Bessel function weights, the true arrival time and diffuse character of the energy become obvious.

We present the derivation of the algorithm, closely following the notation of Carcione (2006). Then we compute the result for a dipole buried in a whole space and compare it with the analytical solution to demonstrate the accuracy of the method. We then apply the scheme to several models to demonstrate its range of application and the wave-like character of the Chebyshev polynomials.

Theory

We follow the development and notation of Carcione (2006), but extend Carcione's two-dimensional (x,z) analysis for dipole magnetic sources to three dimensions (x,y,z) for an electric dipole source. The electric field vector $\mathbf{E}(x,y,z,t)$ satisfies the diffusion equation

$$\frac{\partial \mathbf{E}}{\partial t} = -\frac{1}{\mu\sigma}\nabla\times\nabla\times\mathbf{E} - \sigma\frac{\partial \mathbf{J}}{\partial t} \tag{1}$$

in which $\mu = \mu_0 = 4\pi 10^{-7}$ H/m is the magnetic permeability, σ (S/m) is the electrical conductivity, and **J** is the current source. Carcione (2006) recognized that equation (1) is of the form

$$\frac{\partial \mathbf{w}}{\partial t} = \mathbf{G}\mathbf{w} + \mathbf{s} \tag{2}$$

where w is the wavefield (the electric or magnetic field), ***s*** is the source term, and the 3D operator

$$\mathbf{G} = -\frac{1}{\mu\sigma}\nabla\times\nabla = -\frac{1}{\mu\sigma}\begin{pmatrix} -\left(\partial_y^2+\partial_z^2\right) & \partial_y\partial_x & \partial_z\partial_x \\ \partial_x\partial_y & -\left(\partial_x^2+\partial_z^2\right) & \partial_z\partial_y \\ \partial_x\partial_z & \partial_y\partial_z & -\left(\partial_y^2+\partial_y^2\right) \end{pmatrix}. \tag{3}$$

After discretization, the solution of equation (2) satisfying the initial condition $\mathbf{w}(0) = \mathbf{w}_0$ is formally given by (Carcione 2006, eq. 18):

10.1190/segam2018-2995831.1

$$\mathbf{w}_N(t) = \exp(t\mathbf{G}_N)\mathbf{w}_N^0 + \int_0^t \exp(\tau\mathbf{G}_N)\mathbf{s}_N(t-\tau)d\tau \qquad (4)$$

Using the Chebyshev expansion of $\exp(x)$, in the absence of sources, the discrete solution (Carcione 2006) is

$$\mathbf{w}_N^M(t) = \sum_{k=0}^{M} b_k(t) T_k(\mathbf{F}_N)\mathbf{w}_N^0 \text{, where} \qquad (5)$$

$$\mathbf{F}_N = \frac{1}{a}\left(\mathbf{G}_N + a\mathbf{I}\right), \qquad (6)$$

$\mathbf{I}$ is the identity matrix of dimension 3, and a is the absolute value of the eigenvalue of matrix $\mathbf{G}_N$ having the largest negative real part (See Carcione, 2006). Here

$$b_k(t) = c_k \exp(-at) I_k(at), \qquad (7)$$

$c_0 = 1$, $c_k = 2$, for $k \geq 1$, and I_k is the modified Bessel function. The value of $T_k(\mathbf{F}_N)\mathbf{w}_N^0$ is computed using the recurrence relation for Chebyshev polynomials,

$$T_k(u) = 2uT_{k-1}(u) - T_{k-2}(u), \; k \geq 2, \text{ and} \qquad (8)$$

$$T_0(u) = 1, \; T_1(u) = u, \qquad (9)$$

(Abramowitz and Stegun, 1972, and Carcione, 2006). The maximum wavenumber components are the Nyquist wavenumbers, which for grid spacings Δx, Δy and Δz are $k_x = \pi/\Delta x$, $k_y = \pi/\Delta y$ and $k_z = \pi/\Delta z$. They are related to the highest harmonic of the spatial Fourier transform. Hence, the value of a is

$$a = \frac{\pi^2}{\mu\sigma_{min}}\left(\frac{1}{\Delta x^2} + \frac{1}{\Delta y^2} + \frac{1}{\Delta z^2}\right), \qquad (10)$$

where $\sigma_{\min}$ is the lowest value of conductivity in the model. a has units of s^{-1}. As Tal-Ezer (1989, eq. 4.13) shows, the polynomial order should be $O(\sqrt{at})$. Carcione (2006) found that

$$M = \beta\sqrt{at} \qquad (11)$$

is enough to obtain stability and accuracy, with β in the range 5 to 6. As an initial field we use the time derivative of the analytic expression for the step response of an x-directed dipole at the origin of a full-space, given by Ward and Hohmann (1987). For a source at the origin, the impulse response initial field is then

$$\mathbf{w_0} = \frac{M\sigma^{1/2}\mu^{3/2}}{8\pi^{3/2}t^{5/2}}\exp\left(-\frac{\mu\sigma r^2}{4t}\right)\left[\left(1-\frac{\mu\sigma}{4t}\left(y^2+z^2\right)\right)\mathbf{u_x} + \frac{\mu\sigma xy}{4t}\mathbf{u_y} + \frac{\mu\sigma xz}{4t}\mathbf{u_z}\right]$$

with M the dipole moment, $\mathbf{u_x}$, $\mathbf{u_y}$ and $\mathbf{u_z}$ unit vectors in the x, y and z directions, and $r = (x^2+y^2+z^2)^{1/2}$.

Full-Space Example

Figure 1 shows the three components of the electric field computed with REM at two positions in the computational homogeneous isotropic cube. Comparison with the analytic response demonstrates the accuracy of the computation

.

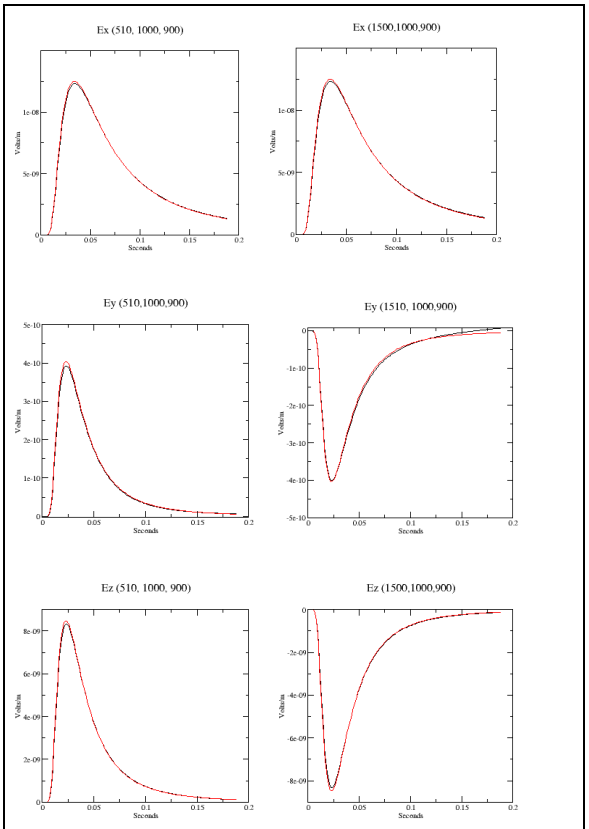

Figure 1 Comparison of pseudo-spectral (black) and analytic (red) responses for E_x, E_y, and E_z components at (510, 1000, 900) on the left and (1500, 1000, 900) on the right. The origin of coordinates is at one corner of the cube. The cube has 200 x 200 x 200 grid points; $\Delta x = \Delta y = \Delta z = 10$ m; the x-directed dipole source is at (1005, 1005, 1005).

10.1190/segam2018-2995831.1

1D Example

Next we compare a reflectivity method (Slob et al., 2010) using the program EMmod described in Hunziker et al. (2015) to the pseudo-spectral REM method. The model is defined on a 400 by 400 by 400 computational grid with a sampling interval of 10 m in each direction. The first 220 samples in depth (2200 m) had a resistivity of 0.3333 ohm-m. From samples 221 to 300 (2210 m to 3000 m) the resistivity increased to 1.0 ohm-m and from sample 301 to 400 (3010 m to 4000 m) the resistivity again increased to 2.0 ohm-m.

The source was an injected analytic Ex dipole at 0.5 ms located almost at the center of the grid, but evaluated for an origin of 2005 m, 2005 m, 2005 m. The receivers were located at all *x* grid positions and for a *y* line at 2000 m. The receivers were at a depth of 2100m. This places them about midway in depth between the source and first reflector. Based on this geometry there should be a direct wave, reflections from the first and second interfaces, and refractions.

Figure 2 shows snap shots for the *x* (upper) and *z* (lower) components of the Chebyshev polynomials, *k*, for the center line, *y* = 2000 m of the 3D computational volume. These snap shots were selected because: (1) the first, at *k* = 200, shows the initial interaction with the first reflector; (2) the second, at *k* = 400, shows this reflection going up towards the receiving array; (3) the third, at *k* = 600, shows it continuing towards the surface; (4) the fourth, at *k* = 800, shows the reflection from the second interface. Note the polarity differences between the *x* and *z* components.

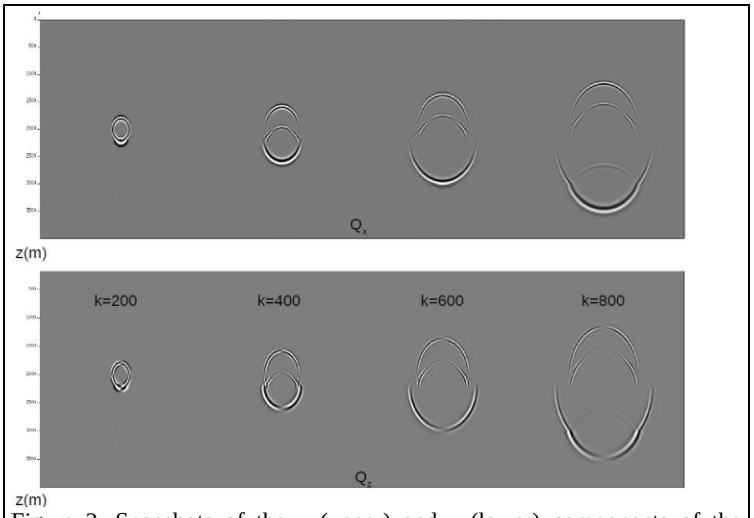

Figure 2. Snapshots of the *x* (upper) and *z* (lower) components of the Chebyshev polynomials, *k* = 200, 400, 600 and 800. Increasing *k* shows the evolution of the electric wave field components and their interactions with the 1st and 2nd reflectors. Note also the polarity of the z component.

We collected the samples of the Chebyshev polynomial for each *k* at the receivers and display them in Figure 3 for positive offsets of 0 to 2000 m. Note the vertical axis is polynomial number *k*. We can see the direct wave, reflections from the two interfaces, and what appears to be a refraction. Since this is a 1D model, the negative source-receiver offset data are identical with the positive offset data for the *x* component.

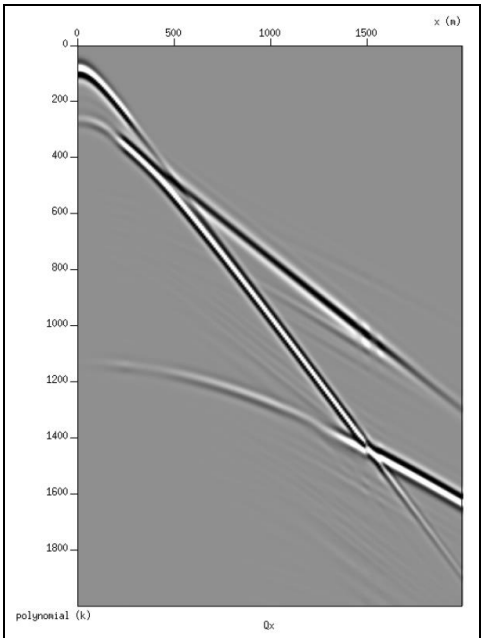

Figure 3. Chebyshev polynomials for the *x* component of the electric field shown for source-receiver offsets of 0 to 2000 m. You can easily identify the direct arrival and reflections from the first and second interfaces. Also visible is a refraction from the second layer. No filtering of any kind was applied to the data and the data were scaled to the maximum amplitude value for display purposes.

10.1190/segam2018-2995831.1

Figure 4 shows the resulting E_x electric wave field data at the receiver positions using the EMmod reflectivity method (left) and the method presented here (right) for the 1D earth model and offsets from 0 to 1000 m shown every 100 m or 10th offset. For comparison, the amplitudes of each trace were normalized to the maximum. No other filtering was applied to the data. The data on the right should be compared with the first half of Figure 3, which are the equivalent Chebyshev polynomials (but for every offset recorded) after integration with the modified Bessel functions. It is clear from the snapshots and the comparison of Figures 3 and 4 that the modified Bessel functions turn the wave-like response of the Chebyshev polynomials into the expected diffuse response of the *E* fields.

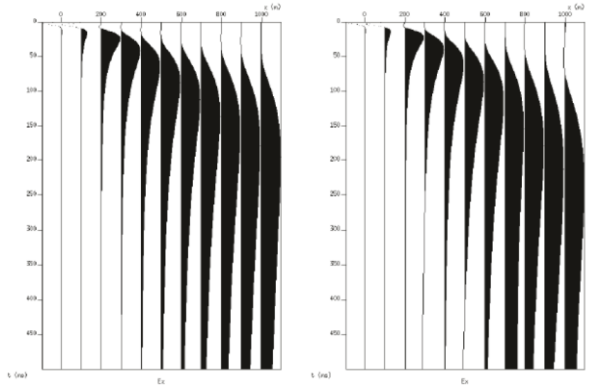

Figure 4. Variable area plot of the E_x simulated data with increasing *x* offset along the source y = 2000 m line. The reflectivity results are shown on the left and the results from the pseudo-spectral REM method are on the right. Every 10th receiver is shown, so the offsets go from 0 to 1000 m. The results are very similar except for the latest arrival times where some differences occur.

3D Example

The basic model was the same as our 1D case, but we introduced a fault block of 50m and removed the second layer from the uplifted fault block. The fault block extends from samples *y* = 191 to 210 (1910 m to 2100 m) and from sample 161 to 190 (1610 m to 1900 m) in *x*.

The source and receiver geometry were the same as for the 1D example. Based on this geometry there should be a direct wave and reflections from the first and second interfaces. But the results of the 3D geometry should show a more complicated set of arrivals, including diffractions and offsets in the arrival times and offsets due to the fault block. Figure5 shows that this is indeed the case

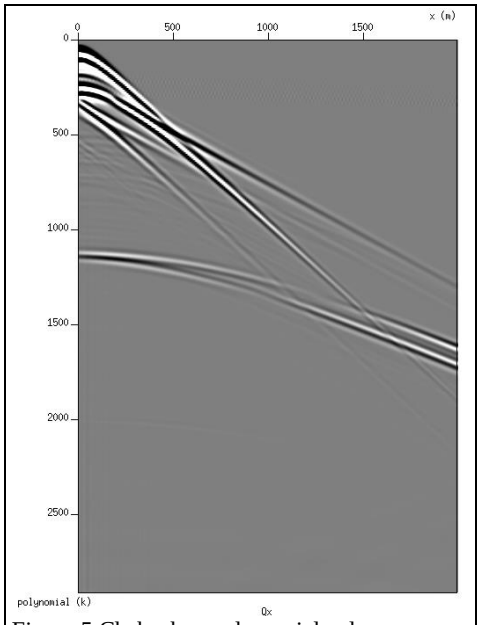

Figure 5 Chebyshev polynomial values collected at the receivers for positive offsets of 0 to 2000 m for the 3D example. Note the vertical axis is polynomial number. We can compare this to the 1D case, Figure 3, and see that we now have a more complicated suite of arrivals.

Conclusions

We have demonstrated that the new flexible 3D three-component full-bandwidth modelling method for transient CSEM data is accurate, by comparing it with the analytic response to a point dipole in a full space. Similar accuracy is obtained in comparisons with 1D modelling. The diffusive field is a weighted sum of Chebyshev polynomials, which exhibit a wave-like character and are very sensitive to small perturbations in the medium. The main advantage of the method is its ability to model 3D electric fields accurately.

The method we developed can be implemented in parallel at two levels. First, each component of the electric field can be computed independently and the updated *E*-field components exchanged only once per polynomial evaluation. Second, within each of these global processes, local parallelism is achieved over all computational loops. This implementation combined with parallel FFTs makes the method computationally feasible.

It is clear from all the examples that it would be easier to interpret and image the Chebyshev polynomials if they could be extracted from the recorded *E* data. This is a topic for future consideration.

10.1190/segam2018-2995831.1

REFERENCES

Abramowitz, M., and I. A. Stegun, 1972, Handbook of mathematical functions: Dover Publications, Inc.

Carcione, J. M., 2006, A spectral numerical method for electromagnetic diffusion: Geophysics, **71**, no. 1, I1–I9, https://doi.org/10.1190/1.2159050.

Fornberg, B., 1987, The pseudo-spectral method: Comparisons with finite differences for the elastic wave equation: Geophysics, **52**, 483–501, https://doi.org/10.1190/1.1442319.

Fornberg, B., 1988, The pseudo-spectral method: Accurate representation of interfaces in elastic wave calculations: Geophysics, **53**, 625–637, https://doi.org/10.1190/1.1442497.

Hunziker, J., J. Thorbecke, and E. Slob, 2015, The electromagnetic response in a layered vertical transverse isotropic medium: A new look at an old problem: Geophysics, **80**, no 1, F1–F18, https://doi.org/10.1190/geo2013-0411.1.

Mittet, R., 2010, High-order finite-difference simulations of marine CSEM surveys using a correspondence principle for wave and diffusion fields: Geophysics, **75**, no. 1, F33–F50, https://doi.org/10.1190/1.3278525.

Pestana, R. C., and P. L. Stoffa, 2010, Time evolution of the wave equation using rapid expansion method: Geophysics, **75**, no. 4, T121–T131, https://doi.org/10.1190/1.3449091.

Slob, E., J. Hunziker, and W. A. Mulder, 2010, Green's tensors for the diffusive electric field in a VTI half-space: Progress in Electromagnetics Research, **107**, 1–20, https://doi.org/10.2528/PIER10052807.

Tal-Ezer, H., 1986, Spectral methods in time for hyperbolic problems: SIAM Journal of Numerical Analysis, **23**, 11–26, https://doi.org/10.1016/S0377-0427(00)00510-0.

Tal-Ezer, H., 1989, Spectral methods in time for parabolic problems: SIAM Journal of Numerical Analysis, **26**, 1–11, https://doi.org/10.1137/0726001.

Ward, S. H., and G. W. Hohmann, 1987, Electromagnetic theory for geophysical applications, *in* M. N. Nabighian, ed., Electromagnetic methods in applied geophysics 1: SEG.